Available online at www.sciencedirect.com

SciVerse ScienceDirect

Journal of the European Ceramic Society 32 (2012) 3423–3434

www.elsevier.com/locate/jeurceramsoc

A quantitative assessment of nanometric machinability of major polytypes of single crystal silicon carbide

Xichun Luo [a,b,*], Saurav Goel [a], Robert L. Reuben [a]

[a] School of Engineering and Physical Sciences, Heriot-Watt University, Edinburgh, EH144AS, Scotland, UK
[b] School of Computing and Engineering, University of Huddersfield HD1 3DH, UK

Received 20 January 2012; received in revised form 3 April 2012; accepted 10 April 2012
Available online 10 May 2012

Abstract

The influence of polymorphism on nanometric machinability of single crystal silicon carbide (SiC) has been investigated through molecular dynamics (MD) simulation. The simulation results are compared with silicon as a reference material.

Cutting hardness was adopted as a quantifier of the machinability of the polytypes of single crystal SiC. 3C-SiC offered highest cutting resistance (∼2.9 times that of silicon) followed by the 4H-SiC (∼2.8 times that of silicon) whereas 6H-SiC (∼2.1 times that of silicon) showed the least. Despite its high cutting resistance, 4H-SiC showed the minimum sub-surface crystal lattice deformed layer depth, in contrast to 6H-SiC. Further analysis of temperatures in the cutting zone and the percentage tool wear indicated that single point diamond turning (SPDT) of single crystal SiC could be limited to either 6H-SiC or 4H-SiC depending upon quality and cost considerations as these were found to be more responsive and amenable to SPDT compared to single crystal 3C-SiC.

Keywords: Nanometric cutting; Ductile regime machining; Tool wear; SiC; Silicon

1. Introduction

Silicon carbide (SiC) has been recognized as a potential candidate for large-scale quantum computing applications, nose covers in Airborne laser (ABL) devices, laser radar systems, vacuum ultraviolet (VUV) telescopes and weather satellites.[1] There is also a growing interest in the use of SiC in the optics industry for space based laser mirrors as a replacement for beryllium.[2] Due to its superior properties, such as high-temperature resistance and chemical inertness, SiC is being actively explored as a future material for advanced semiconductor electronic device applications,[3] leading to a potential demand for cost effective manufacturing of complex SiC components with mirror finish. Davies et al.[4] have quoted Fortune[5] saying that "Ultraprecision machining (UPM) is doing for light what integrated circuits did for electronics".

Single point diamond turning (SPDT) is now an established ultra precision manufacturing method to obtain mirror finish surfaces right up to the edge of the element[6] on a variety of brittle materials.[4,7–10] In fact, the diamond turned optical surface has a better metallurgical structure than that obtained after machining using polishing and lapping processes.[11] Therefore, significant cost reduction can be achieved to produce optical quality and damage-free SiC surfaces through diamond turning as it will require fewer manufacturing steps than grinding, polishing and lapping methods.

SiC exhibits one-dimensional polymorphism, all polytypes having the same planar arrangement of Si and C atoms but different stacking sequences. About 250 polytypes of silicon carbide (SiC) have been recognized by their energetic equivalence demonstrated through theoretical thermodynamic calculations.[12] The two major polymorphs are α-SiC and β-SiC with hexagonal and zinc-blende lattice structures, respectively. The main engineering properties of β-SiC (3C-SiC) and α-SiC (6H-SiC and 4H-SiC) are listed in Table 1, along with the corresponding values for single crystal silicon as a reference material.

It can be seen that the properties of the individual polytypes differ significantly despite the fact that all share the same tetrahedral geometry of silicon and carbon atoms as shown in Fig. 1.

* Corresponding author. Tel.: +44 0 1314513197; fax: +44 0 1314513129.
E-mail address: x.luo@hud.ac.uk (X. Luo).

0955-2219/$ – see front matter © 2012 Elsevier Ltd. All rights reserved.
http://dx.doi.org/10.1016/j.jeurceramsoc.2012.04.016

Table 1
Engineering properties of polytypes of SiC and silicon.

Parameter	3C-SiC	4H-SiC	6H-SiC	Silicon
Experimental lattice parameter (Å)	$a = 4.359$[13]	$a = 3.079$[13] $c = 10.254$[13]	$a = 3.0817$[13] $c = 15.1183$[13]	5.43[14]
Mechanical properties				
Bulk modulus (K) (GPa)	225[15]	215[16]	215[16]	98[17]
Shear modulus (G) (GPa)	124[18]	131.4[18]	131.4[18]	79.9[18]
Hardness (H) on (1 0 0) plane (GPa)	25–30[16]	26[20]	20–26[21]	9.8[19]
Poisson's ratio (υ)	0.267[18]	0.231[18]	0.231[18]	0.27[18]
Young's modulus (E) (GPa) "$E = 3K(1-2\upsilon)$"	314.55	347.01	347.01	135.24
Fracture toughness (K_c) (MPa m$^{1/2}$)	2.02[22] 3.23 for CVD	1.9[23]	1.9[23]	0.9[24]
Electronic properties [25–29]				
Band gap (eV)	2.3	3.2	3	1.1
Hole mobility (cm^2/V.s)	40	115	90	420
Electron mobility (cm^2/V.s)	750	//c-axis: 800 ⊥ c-axis: 800	//c-axis: 60 ⊥ c-axis: 800	1200
Thermal conductivity (W/cm-K)	4.9	3–5	3–5	1.5
Electron saturation velocity (cm/s × 10^7)	2.5	2	2	1
Breakdown electric field strength (V/cm × 10^6)	1.8	//c-axis: 3 ⊥ c-axis: 2.5	//c-axis: 3.2 ⊥ c-axis: >1	0.6

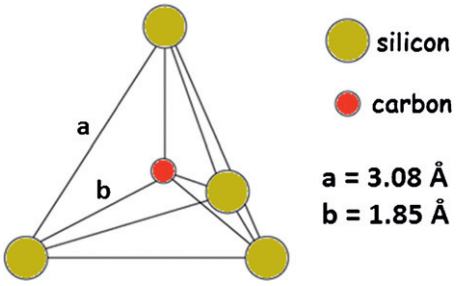

Fig. 1. Tetrahedral geometry of SiC.

This difference in material properties of various polytypes of SiC is fundamentally attributable to the difference in the stacking arrangement of SiC bilayers along the c-axis of β-SiC and along the (0 0 1) direction of α-SiC.[30] Fig. 2 shows the stacking sequence of silicon and carbon atoms in various polytypes of SiC.

It can be seen from Fig. 2 that, if the first Si-C layer is labelled A, a close packed structure can be obtained placing the next layer at either of positions B or C. The various polytypes of SiC are simply permutations of three such positions. Thus defined, the stacking sequence is ABC in 3C-SiC, ABCB in 4H-SiC and ABCACB in 6H-SiC. Although, SPDT of 6H-SiC,[31,32] CVD(polycrystalline) 3C-SiC,[1] RB-SiC[10] and 4H-SiC[33] has

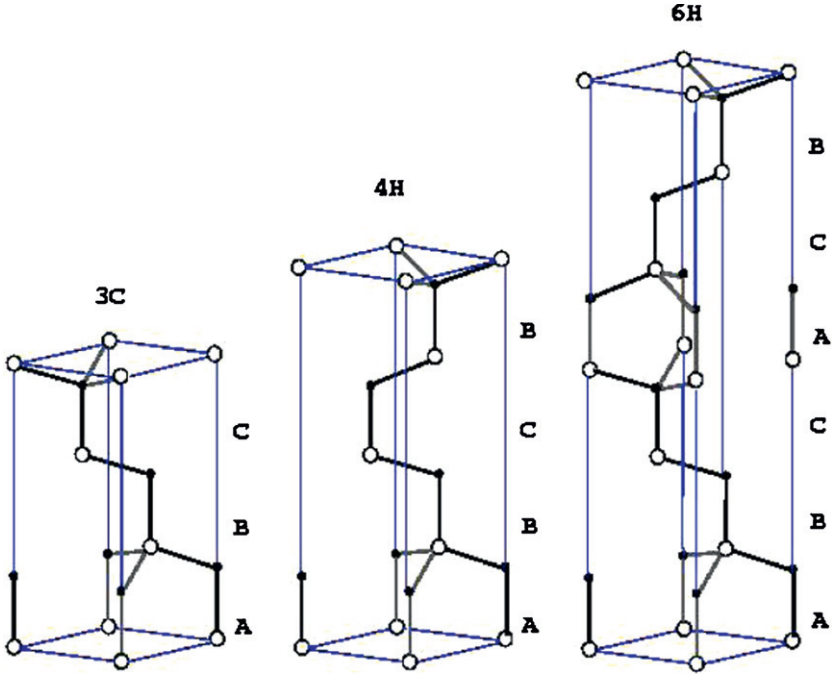

Fig. 2. Stacking sequence of bilayers in polytypes of SiC.[28]

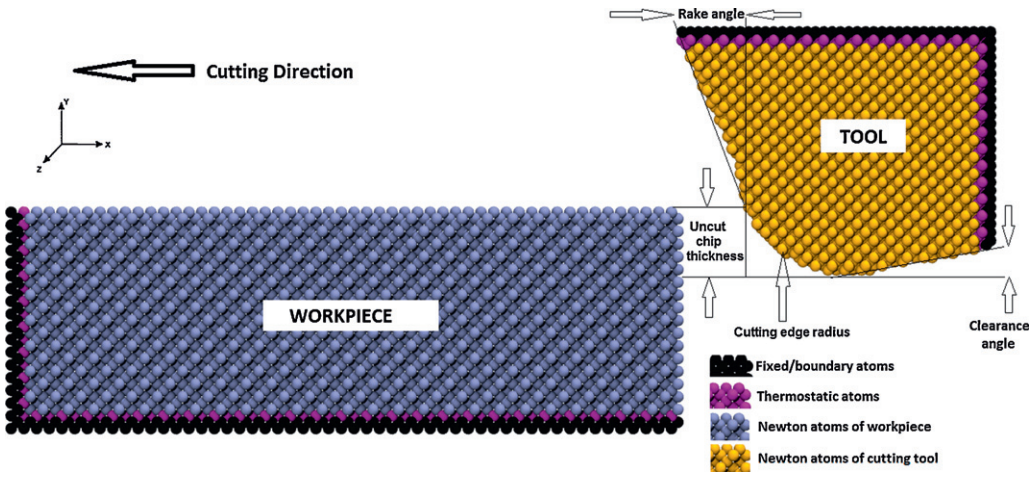

Fig. 3. Schematic of MD simulation model.

been successfully demonstrated, a theoretical study at a fundamental atomic level will answer some key questions which are difficult to observe on-line during experiments. For example, it is important to know if it is possible to generate defect-free surfaces in all the major polytypes of single crystal silicon carbide, and, if so, under what machining conditions. Also, it is of interest to know if some polytypes are more amenable to SPDT. Hence, it is worthwhile to simulate the SPDT mechanism for all polytypes of SiC simultaneously, which is the key motivation for the current work to characterize quantitatively the nanometric machinability and investigate the feasibility of SPDT for various polytypes of SiC in a way that is indexed to silicon, which is comparatively well-studied.

This is an important precursor to experimental studies, which would not only be expensive, but would also not permit direct observation of all the events occurring at the atomic level, which normally take place over timescales in the femtosecond range. Not every simulation method is suitable for this application; for example, the classical theory of finite element method (FEM) assumes the material to behave as a continuum whereas the relevant atomic level phenomena are discrete.

If, as suspected, the key to such processes lies in understanding the atomic level events, MD should be an appropriate simulation approach, as it is one which has already been successful in addressing a number of key problems concerning nanometric cutting processes.[34–38] The relatively slow computational speed can be overcome using the quasi-continuum (QC) multi-scale simulation method[39] which harnesses the combined advantages of both MD and FEM. However, QC software is yet to be developed to simulate silicon-like complex diamond cubic lattices. Considering the above limitations, this paper adopts a state-of the-art MD simulation employing a suitable three-body potential energy function for describing the SPDT of various polytypes of SiC alongside silicon as a reference material.

2. MD simulation

A public-domain computer code, known as "Large-scale atomic/molecular massively parallel simulator" (LAMMPS)[40] was used to perform the MD simulation. The following paragraphs give details of the implementation of this code for the simulation in hand.

2.1. MD simulation model

A schematic diagram of the nanometric cutting simulation model is shown in Fig. 3. Both the single-crystal SiC workpiece and the diamond cutting tool have been modelled as deformable bodies in order to study the tribological interactions between the two. This is in contrast to previous simulations which have taken the cutting tool to be a rigid body, a reasonable assumption if the focus of interest is the mechanism of nanometric cutting rather than the tool wear.[41–43] The model developed in this work is based on the boundary condition of bottom and closed cut out side which was found more appropriate to study nanometric cutting process.[44] Also, the MD model incorporates a negative tool rake angle, as this is generally recommended for machining brittle materials. [45] The atoms of both cutting tool and workpiece were allocated into one of the three different zones: Newton atoms, thermostatic atoms and boundary atoms.

The essence of nanometric cutting simulation through MD is simply a classical solver of Newton's second law of motion, where the atoms in the Newton and thermostatic zones are assumed to follow Newton's second law as follows:

$$a_{ix} = \frac{F_{ix}}{m_i} = \frac{d^2x_i}{dt^2} \quad , \quad F_{ix} = -\frac{dV}{dx_i} \tag{1}$$

where a_{ix} represents the ith atom's acceleration in the x direction and m_i is the mass of the ith atom. F_{ix} is the interaction force acting on the ith atom by the jth atom in the x direction, x_i is ith atom's x-coordinate and V is the potential energy function.

The boundary atoms are assumed to remain unaffected during the simulation and thus remain fixed in their initial lattice positions, serving to reduce the boundary effects and maintain the symmetry of the lattice. In conventional machining operations, the energy from plastic deformation in the primary shear zone and friction at the tool–chip interface generate heat, which is carried away by chips and lubricant and by conduction into the

tool and workpiece. The nanometric cutting model is, however, extremely small and is not capable of dissipating the cutting heat itself. The motion of the thermostatic atoms is therefore re-scaled to a temperature of 300 K at every time step. The velocity of the atoms can be used to compute the local temperature of the atoms using the relationship between kinetic energy and temperature:

$$\frac{1}{2}\sum_i m_i v_i^2 = \frac{3}{2}Nk_bT \tag{2}$$

where N is the number of atoms, v_i represents the velocity of ith atom, k_b is the Boltzmann constant ($1.3806503 \times 10^{-23}$ J/K) and T represents the atomistic temperature. However, the instantaneous fluctuations in kinetic energy per atom would be very high so these are averaged temporally and/or spatially over few timesteps and reassigned to each atom at every N steps to be converted into equivalent temperature. It should be noted here that the movement of the tool will also contribute to the kinetic energy so the component of tool displacement should accordingly be subtracted.

2.2. Potential energy function

A potential energy function fundamentally governs the accuracy and reliability of the results obtained from the MD simulation. Hence, an appropriate potential function for silicon and carbon interactions must be chosen. The Tersoff potential function, being a three-body potential function, can provide a more realistic description of covalent bonded materials like silicon and carbon, so it was used to describe Si–Si, C–C and Si–C interactions as follows:

$$E = \sum_i Ei = \frac{1}{2}\sum_{i \neq j} V_{ij}$$
$$, \quad V_{ij} = fc(r_{ij})[f_R(r_{ij}) + b_{ij} f_A(r_{ij})] \tag{3}$$

Table 2
Tersoff potential parameters.[46,47]

	Si–Si	C–C
A (eV)	1830.8	1393.6
B (eV)	471.18	346.74
λ (Å^{-1})	2.4799	3.4879
μ (Å^{-1})	1.7322	2.2119
β	1.1×10^{-6}	1.5724×10^{-7}
n	0.78734	0.72751
c	1.0039×10^{5}	3.8049×10^{4}
d	16.217	4.3484
h	−0.59825	−0.57058
R (Å)	2.7	1.8
S (Å)	3	2.1
$\chi_{Si–C}$	0.9776	

$$f_R(r_{ij}) = A_{ij}\exp(-\lambda_{ij}r_{ij}) \quad , \quad f_A(r_{ij}) = -B_{ij}\exp(-\mu_{ij}r_{ij}) \tag{4}$$

$$fc(r_{ij}) = \begin{cases} 1 & r_{ij} < R_{ij} \\ \frac{1}{2} + \frac{1}{2}\cos\left[\pi\left(\frac{r_{ij} - R_{ij}}{S_{ij} - R_{ij}}\right)\right] & S_{ij} > r_{ij} > R_{ij} \\ 0 & r_{ij} > S_{ij} \end{cases} \tag{5}$$

$$b_{ij} = \chi_{ij}(1 + \beta_i^{ni}\zeta_{ij}^{ni})^{-1/2n_i} \quad , \quad \zeta_{ij} = \sum_{k \neq i,j} fc(r_{ik})\omega_{ik}g(\theta_{ijk}) \tag{6}$$

$$g(\theta_{ijk}) = 1 + \frac{c_i^2}{d_i^2} - \frac{c_i^2}{[d_i^2 + h_i - \cos\theta_{ijk}]} \tag{7}$$

Table 3
Process variables used for MD simulation model.

Workpiece material	Number of atoms in the workpiece	Number of atoms in the diamond cutting tool
3C–SiC (14.2624 nm × 4.6353 nm × 4.2787 nm)	28600	21192
6H–SiC (14.2624 nm × 4.6353 nm × 5.1347 nm)	31999	25607
4H–SiC (14.2624 nm × 4.6353 nm × 3.92216 nm)	27360	19426
Silicon (14.2624 nm × 4.6353 nm × 4.2787 nm)	14840	21192
Equilibrium lattice parameters used for the workpiece (Å)		
$a = b = c = 4.321$; $\alpha = \beta = \gamma = 90^\circ$		3C–SiC
$a = b = 3.07$; $c = 14.26$; $\alpha = \beta = 90^\circ$; $\gamma = 120^\circ$		6H–SiC
$a = b = 3.07$; $c = 9.856$; $\alpha = \beta = 90^\circ$; $\gamma = 120^\circ$		4H–SiC
$a = b = c = 5.432$; $\alpha = \beta = \gamma = 90^\circ$		Silicon
Crystal orientation of diamond tool		Cubic
Crystal orientation of workpiece		(010)
Cutting direction		<1 0 0>
Cutting edge radius (nm)		2.2974
Uncut chip thickness/in-feed (nm)		1.3128
Cutting tool rake and clearance angle		−25° and 10°
Equilibration temperature		300 K
Cutting velocity		100 m/s
Timestep		0.5 fs

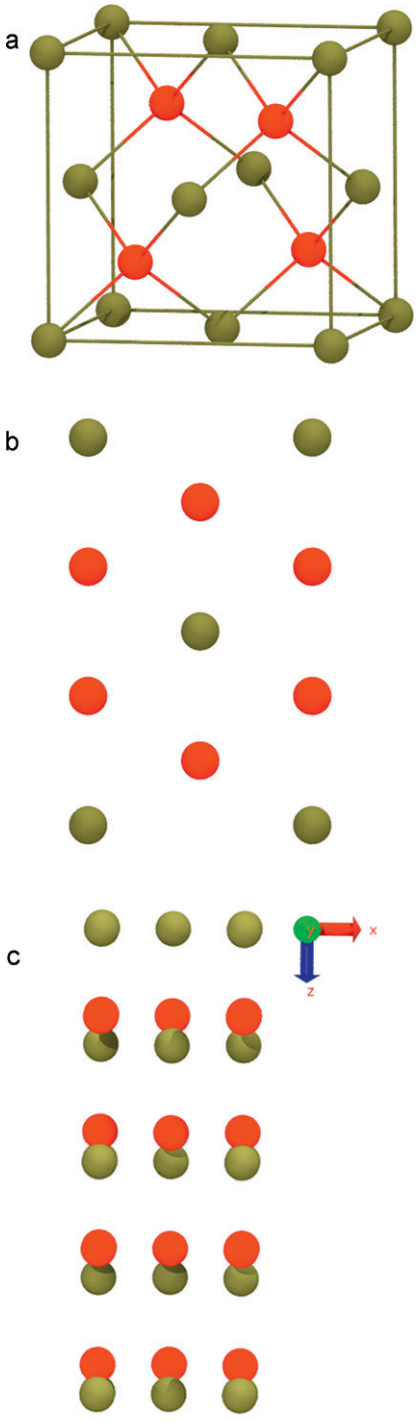

Fig. 4. Unit cell of SiC. (a) Orthographic view, β-SiC, (b) view onto (0 0 1) plane, α-SiC, (c) view onto (1 0 0) plane, α-SiC.

where E_i is the site energy, the sub-function, V_{ij} describes the energy between two atoms (i and j), (i, j and k) label the three atoms of the system, f_R represents a repulsive pair potential, f_A represents an attractive pair potential, f_C represents a smooth cut-off function to limit the range of the potential, r_{ij} is the length of the i–j bond, b_{ij} is the bond order term, ζ_{ij} counts the number of other bonds to atom i besides the i–j bond, θ_{ijk} is the bond angle between the bonds i–j and i–k and $\chi_{Si–C}$ is the mixing parameter.

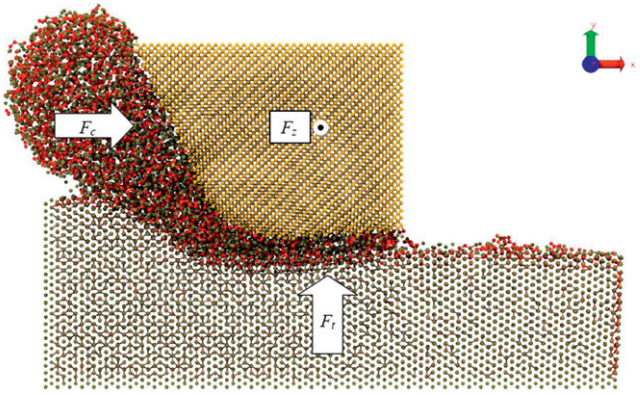

Fig. 5. Cutting forces during nanometric cutting (a) thrust forces and (b) cutting forces.

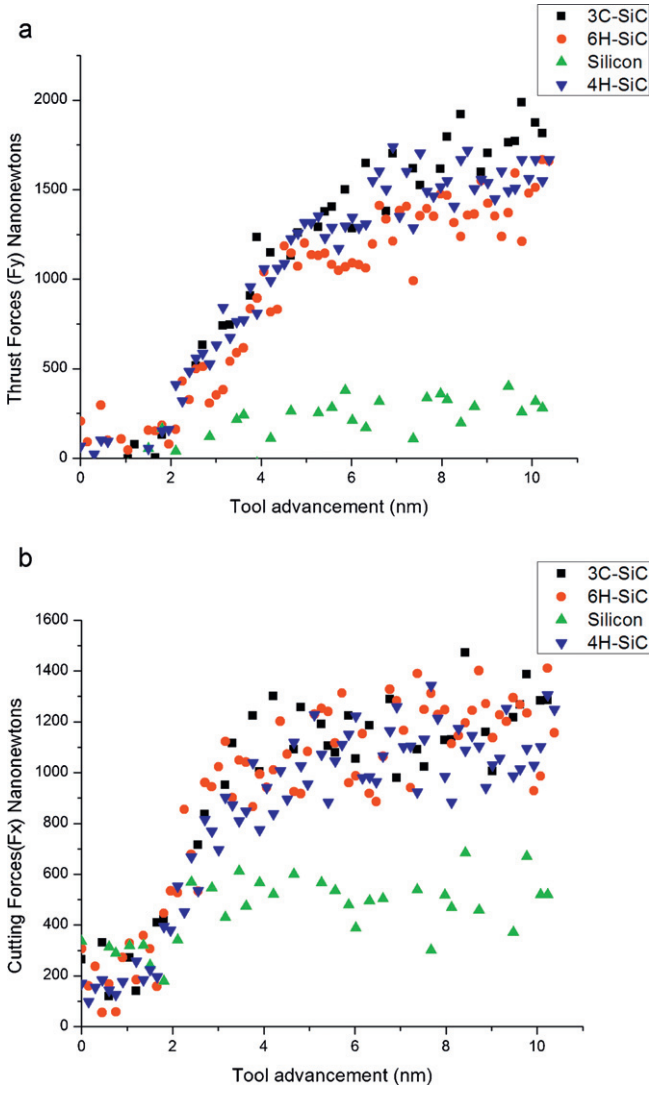

Fig. 6. Comparison of thrust and cutting forces during nanometric cutting.

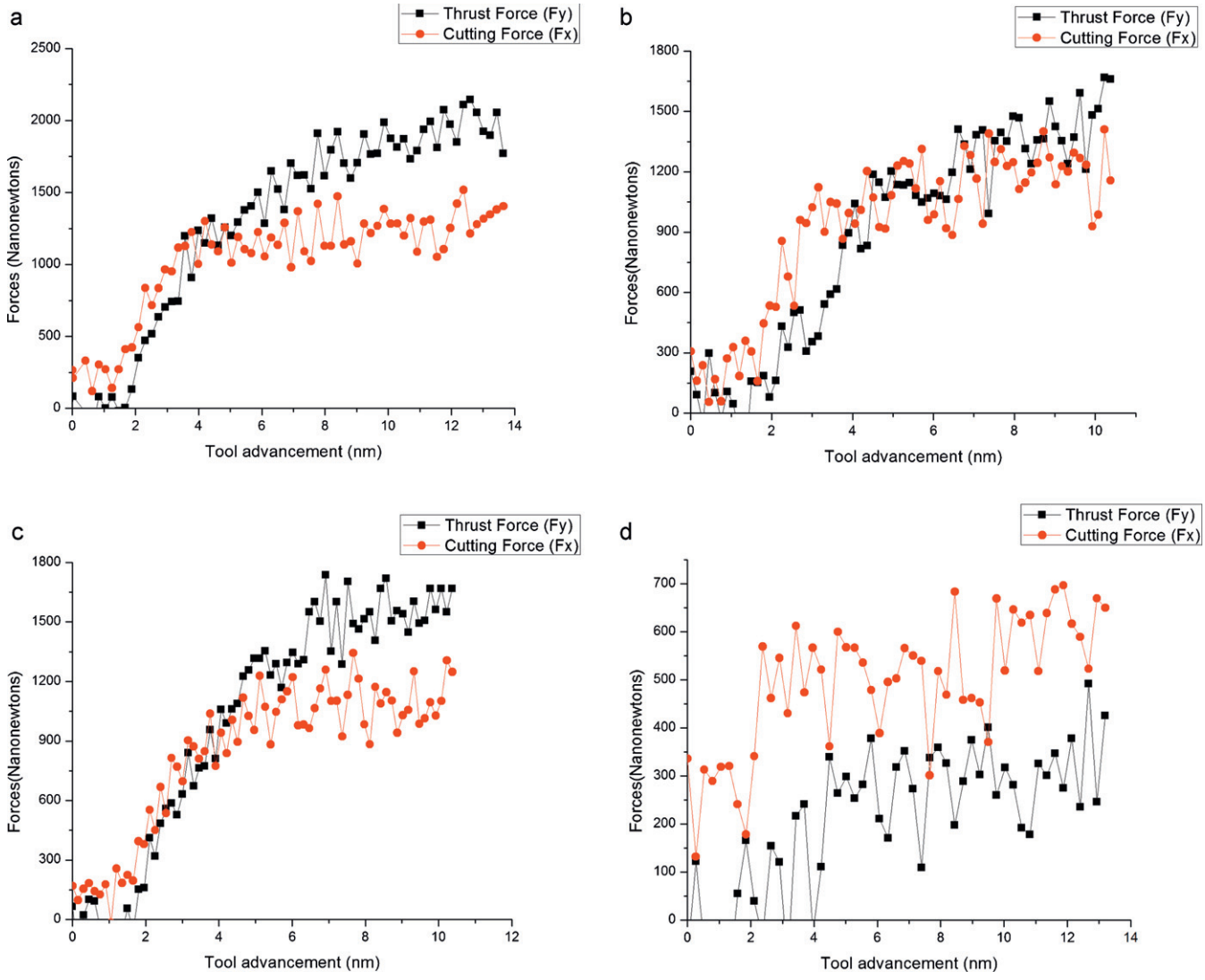

Fig. 7. Comparison of forces on individual material during nanometric cutting (a) 3C-SiC, (b) 6H-SiC, (c) 4H-SiC, (d) silicon.

The potential function parameters and process variables which were used in the current MD simulation model are listed in Tables 2 and 3.

2.3. MD simulation setup

The MD simulation model was developed by replicating the unit cell using periodic boundary conditions. This was followed by energy minimization to avoid overlaps in the positions of the atoms. The simulation model was equilibrated to 300 K under the micro canonical (NVE) ensemble and the initial velocities of the atoms were assigned in accordance with a Maxwell–Boltzmann distribution. During the equilibration process, the total energy is not conserved and so the trajectories must not be used to compute any properties while the potential energy continues to convert to kinetic energy and *vice-versa*. This procedure causes the temperature to fluctuate until it becomes stationary. Once sufficient time has been given for equilibration, the velocity scaling is

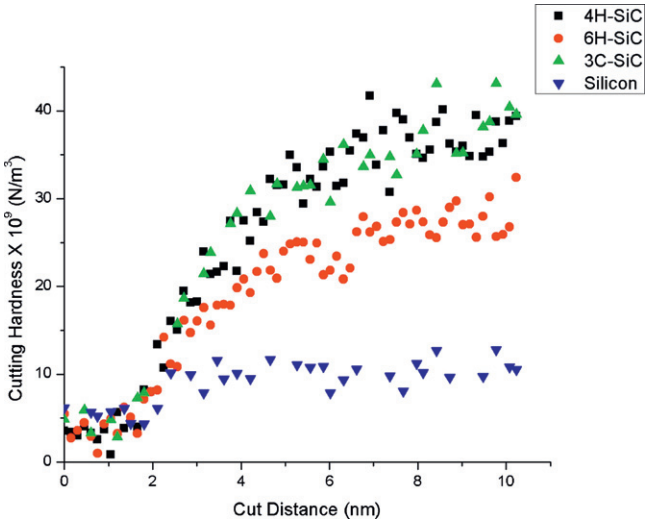

Fig. 8. Cutting hardness of various polytypes of SiC compared with silicon.

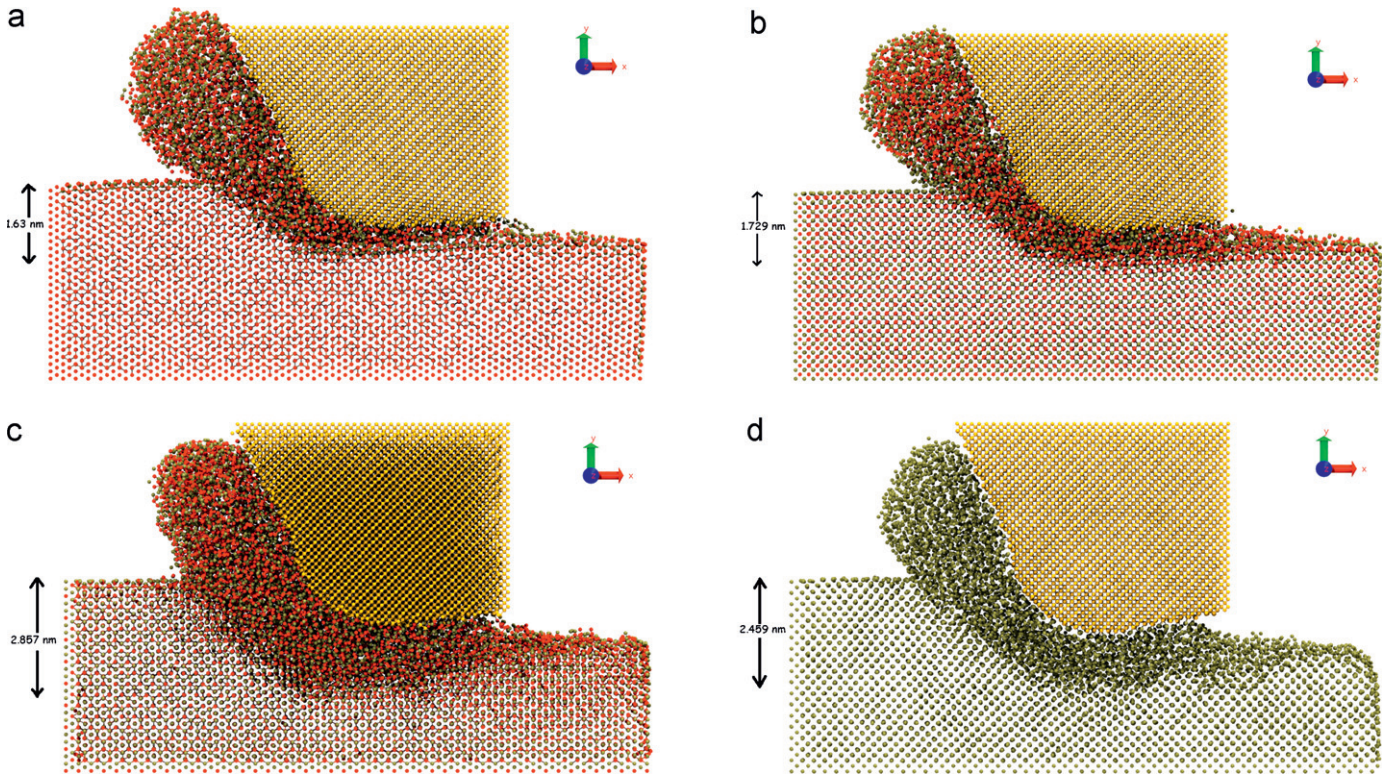

Fig. 9. (a) Sub-surface crystal lattice deformed layer depth and chip morphology of 4H-SiC. (b) Sub-surface crystal lattice deformed layer depth and chip morphology of 3C-SiC. (c) Sub-surface crystal lattice deformed layer depth and chip morphology of 6H-SiC. (d) Sub-surface crystal lattice deformed layer depth and chip morphology of silicon.

removed and the system then follows NVE dynamics. Different views of the unit cell of SiC are shown in Fig. 4 where the green and red colours[1] correspond to silicon and carbon atoms respectively. Visual Molecular Dynamics (VMD) software[48] was used for enhanced visualization of atomistic data.

3. Results and discussions

This section covers observations and discussion of the significance of the MD simulations in terms of the cutting forces, cutting hardness, chip morphology, workpiece deformation, temperature in the cutting zone and, finally, the tool wear.

3.1. Cutting forces and cutting hardness

Fig. 5 shows schematically the orientation of the components of cutting force acting on the tool. The "cutting force" (F_c) acts in the x direction, the "thrust force" (F_t) acts in the y direction and F_z acts in the direction orthogonal to the X and Y planes. A comparison of the main components (thrust and cutting forces) for all the simulations is shown in Fig. 6.

It can be seen from Fig. 6 that the magnitudes of the forces are significantly higher for all polytypes of SiC compared to silicon and, as with the thrust force (F_y), the highest in magnitude is for 3C-SiC, followed by 4H-SiC and 6H-SiC in that order. The magnitudes of the cutting forces (F_x) were however, found to be in a different order, the highest being for 3C-SiC, followed by 6H-SiC and 4H-SiC.

Fig. 7 shows an individual comparison of thrust and cutting force development for each material. It seems that the cutting forces (F_c) are higher than the thrust forces (F_t) for machining silicon, whereas the reverse is the case for SiC. In conventional cutting, the dominance of cutting forces over thrust forces is attributed to the larger shear plane area which results from a decrease in shear angle.

The magnitude and nature of the thrust and cutting forces observed in 3C-SiC here are in close agreement with another MD simulation study which used the ABOP formalism based potential energy function.[49] Patten and Gao[50] have demonstrated that increasing the negative tool rake angle will increase the thrust force (F_y) compared to the cutting force (F_x) during SPDT. It is of further interest to note that higher cutting forces were observed while cutting 6H-SiC with a tool having a negative rake angle of -45°.[31] However, the cutting tool deployed had a very large clearance angle (40°) and hence it experienced lower thrust forces than cutting forces. Neither thrust force nor cutting force in the current case is a clear criterion to assess the relative machinability of the material. The difficulty in evaluation of the machinability of the material can, however, be overcome using the "cutting hardness", which has been suggested[51] as a quantitative indicator of the cutting resistance of

[1] Readers are referred to the web based version of this article to interpret the correct colour legends.

a material irrespective of the machining parameters, expressed as follows:

$$\text{Average cutting hardness} = \frac{\text{resultant force}}{\text{volume of material removed}} = \frac{\sqrt{Ft^2 + Fc^2}}{bdl} \quad (8)$$

where F_t and F_c are the thrust and cutting forces, respectively, b is the width or depth of cut, d is the uncut chip thickness and l is the length of cut. The evolutions of cutting hardness for 3C-SiC, 4H-SiC, 6H-SiC are shown in Fig. 8, compared with the reference material, silicon.

The average values of cutting hardness over the 10 nm tool advancement for silicon, 3C-SiC, 6H-SiC and 4H-SiC were found as 9.1, 26.4, 19.2 and 25.5 respectively, so 3C-SiC offered the highest cutting resistance (~2.9 times that of silicon) followed by 4H-SiC (~2.8 times silicon) and 6H-SiC (~2.1 times silicon).

The ratios of transition pressure and cutting hardness were found to be 2.25, 2.15, 1.75 and 1.42 for 6H-SiC, 3C-SiC, 4H-SiC and silicon respectively. A study made during the 1970s reported this ratio in carborundum as 1.69[52] and looks in reasonable agreement with the value of 1.75 obtained for 4H-SiC.

3.2. Chip morphology and sub-surface crystal lattice deformed layer depth

The sub-surface damage thickness is critical information at each step of the manufacturing process. Monnoye et al.[53] have indicated that different experimental methods e.g. Normarski observation, transmission electron microscopy, Rutherford backscattering, photon backscattering, KOH etching, Raman scattering and even positron annihilation have been used to identify the sub-surface deformation layer depth. Since all the machining parameters in the current simulation were kept the same, the sub-surface deformation will give a useful relative measure for the individual polytypes. Moreover, chip morphology and subsurface deformation are of critical interest because they govern the obtainable surface finish and form accuracy. In the current simulation, although, both SiC and silicon show curly chip formation, the extent of this varies and the finished surface and subsurface obtained after machining differs significantly. Thus, severe plastic deformation, compounded with high pressure underneath the tool, results in alteration of the microstructure in the sub-surface of the machined component. Depending upon the characteristics of the sub-surface, this may influence component life by its effect on residual stress, fatigue and creep. The chip shapes in Fig. 9 show that chip formation has taken place in all four materials by deformation rather than fracture, i.e. that ductile-regime machining could be achieved.

Fig. 9 also shows an estimate of the sub-surface deformation depth below the uncut surface directly under the tool position for all the polytypes of SiC and silicon. The quality of the finished surface (indicated by the deformed layer depth) appears

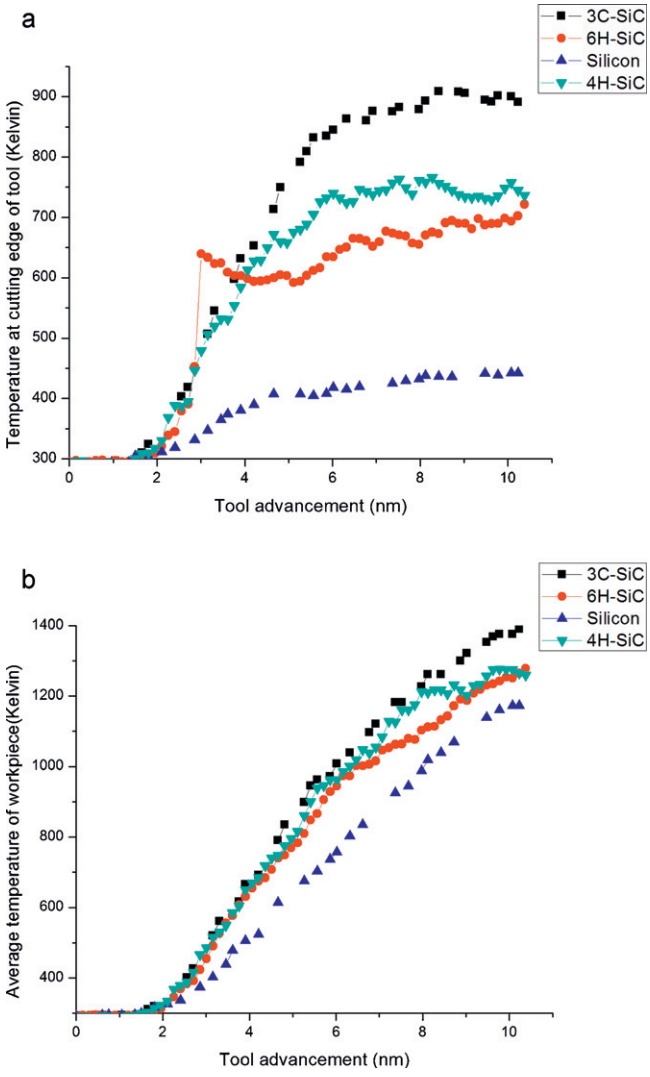

Fig. 10. Comparison of temperature evolutions during nanometric cutting.

to be the best obtained on 4H-SiC, followed by 3C-SiC, silicon and, finally, 6H-SiC whose sub-surface is heavily distorted. This can be quantified by subtracting the uncut chip thickness from the estimate shown in Fig. 9, giving maximum sub-surface deformed layer depths from the finished surface of 0.32 nm, 0.42 nm, 1.54 nm and 1.15 nm accounting for about 1.24, 1.32, 2.18 and 1.87 times the uncut chip thickness for 4H-SiC, 3C-SiC, 6H-SiC and silicon, respectively.

Experimental measurement of sub-surface deformation depth is time consuming and difficult. Whereas the nanometric cutting and nano-indentation processes differs [54], the sub-surface deformation measured experimentally during nano-indentation on 6H-SiC, found to be 2.5 times the maximum indentation depth [55] provides further evidence that 6H-SiC is apt to undergo large sub-surface deformations during contact loading. To further confirm these findings, the critical crack length, which is dependent on the fracture toughness and hardness has been calculated as shown in Table 4.

Amongst the polytypes, 3C-SiC has the maximum fracture toughness and maximum hardness while 6H-SiC has the

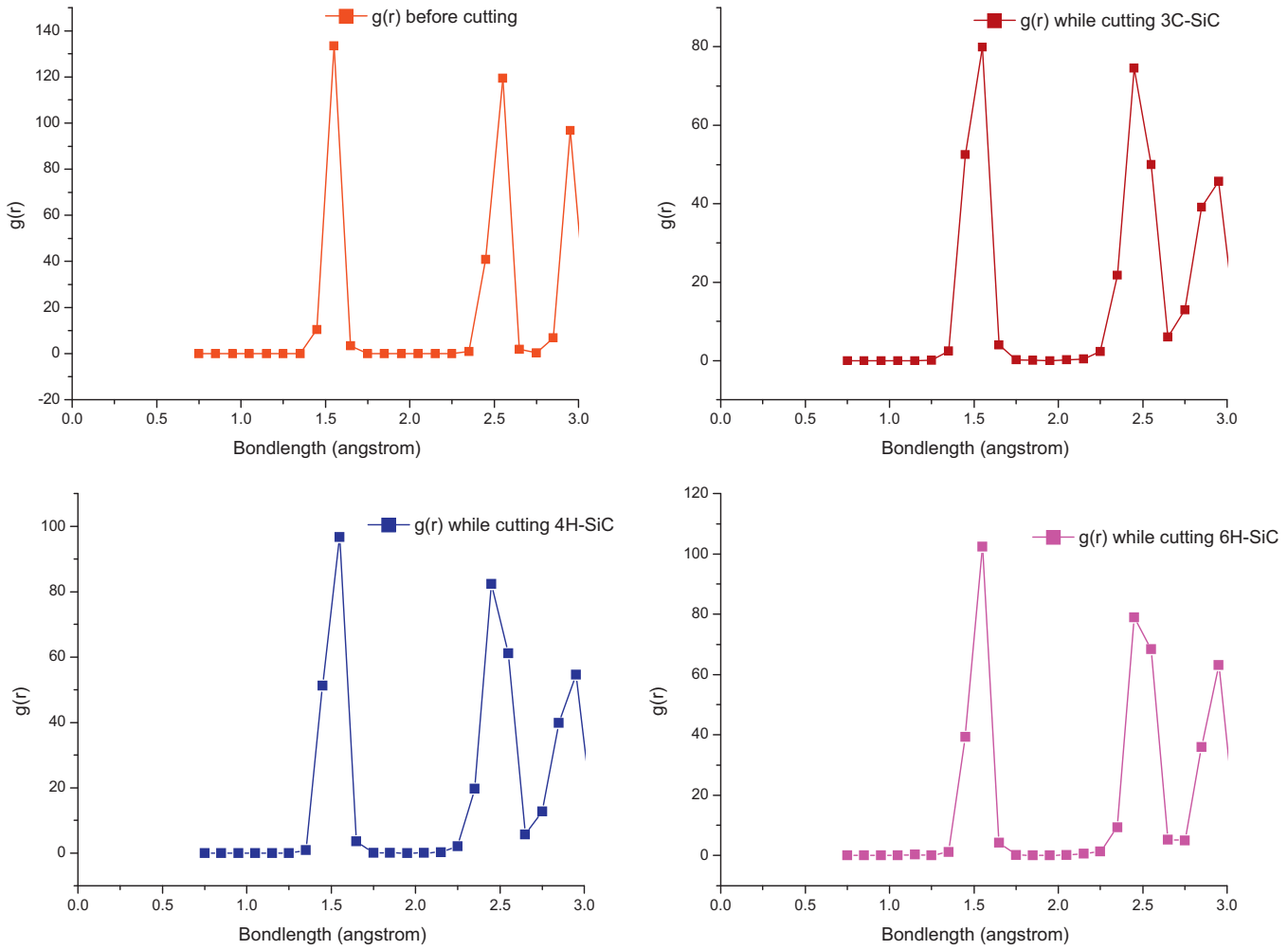

Fig. 11. Radial distribution function of diamond tool against various polytypes of SiC.

least hardness and shares the same fracture toughness as 4H-SiC. The ductile regime machining model [58] assumes that fracture damage starts at a critical chip thickness so that smaller critical crack lengths are desirable in order that a crack free machined surface is obtained making 4H-SiC the preferred choice over other polytypes for SPDT. Thus, both MD and the ductile regime machining model suggest that 6H-SiC give the poorest and 4H-SiC the best surface conditions.

It is interesting to note that, despite the differences between the nano-indentation process and nanometric cutting processes, it's a similar ductile response is found for silicon in both[59–61], which occurs by the virtue of high pressure phase transformation (HPPT). In contrast to silicon, silicon carbide has been reported to give different responses some [62,63] suggesting, for example that 3C-SiC undergoes amorphization and another group suggesting that it transforms from its stable zinc-blende lattice structure to a rocksalt structure [15,64,65]. Similarly, different responses have been reported, for 6H-SiC and 4H-SiC, including transformation to a polycrystalline phase,[55] no high pressure phase transformation[10,66] and dislocation nucleation followed by propagation within the zinc-blende phase.[67] Since, nanometric cutting involves high pressure and moderate temperature[31] in the cutting zone, an sp^3–sp^2 transition right under the wake of the tool was suggested as a mechanism for the ductility of 3C-SiC.[68] This is further consistent with the fact that SiC, in common with

Table 4
Calculation of critical crack length.[56,57]

S. no.	Material	Fracture toughness (MPa $m^{1/2}$) (from Table 1)	Hardness (GPa) (obtained from current simulation)	Critical crack length (μm) $c* = 120\left[\frac{K_c^2}{H^2}\right]$
1	3C-SiC	2.02	26.4	0.7025
2	4H-SiC	1.9	25.5	0.6667
3	6H-SiC	1.9	19.2	1.1751
4	Silicon	0.9	9.1	1.1737

diamond, requires a lower force for bond-bending than bond stretching, the opposite to other typical semi-conductors such as Si, Ge, Si_3N_4 or GeAs.[69,70]

3.3. Temperature during the machining process

Fig. 10 shows the average rise in temperature of the cutting edge of the tool and on the workpiece as the tool moves through each of the workpiece materials.

The 3C-SiC showed the highest temperatures both on the cutting edge and the workpiece followed by 4H-SiC, 6H-SiC and silicon, so that all polytypes of SiC result in higher cutting temperatures than single crystal silicon. A high temperature in the cutting zone reduces the life of diamond tools[37] as it reduces hardness through graphitization of the diamond a process which is accelerated further in the presence of properly directed shear stresses.[71] This mechanism can be examined by analysis of the radial distribution function, as discussed in the next section. High temperatures are, of course, known to compromise the life of diamond tools, and an appropriate coolant may help to ameliorate this and provide improved surface roughness as well.[72,73]

3.4. Tool wear

Wear of diamond tools is undesirable in SPDT not only because of the replacement cost but also because of its effect on the attainable surface finish. In-process degradation of the diamond tool due to wear may alter the tool–workpiece contact and hence the machining conditions which can cause a sudden transition of material removal mechanism from ductile mode to brittle fracture in the cutting region with consequent deterioration in surface finish.

A good understanding of the wear mechanism is an essential step in identifying mitigation measures. Recently, it has been reported that diamond tools undergo graphitization during nanometric cutting of 3C-SiC.[49] However, the root cause of tool wear during nanometric cutting of other polytypes of SiC is still unknown.

It is widely accepted that measurement of the variation in inter-atomic distance during machining simulations gives insights into the wear mechanism. For this purpose, the radial distribution function for diamond tool is plotted before and during nanometric cutting in Fig. 11, which shows that, before cutting, the radial distribution function $-g(r)$ has a peak at 1.54 Å which is the known bond length of diamond[74] while a few bonds on the surface (dangling bonds) result in a small peak (visible as a slight asymmetry of the 1.54 Å peak) at 1.42 Å. During machining, with the continued advancement of the tool, this small peak continues to grow at the expense of the number of atoms with a bond length of 1.54 Å. This observation is common for all the polytypes of SiC but with varying magnitude. The value of 1.42 Å is the known bond length of another stable allotrope of carbon, graphite[75] which is much weaker than diamond due to its chemical structure. Thus, $g(r)$ confirms graphitization of diamond tools during SPDT for all the polytypes of SiC. It is also now known that, while machining silicon, diamond undergoes graphitization in addition to the formation

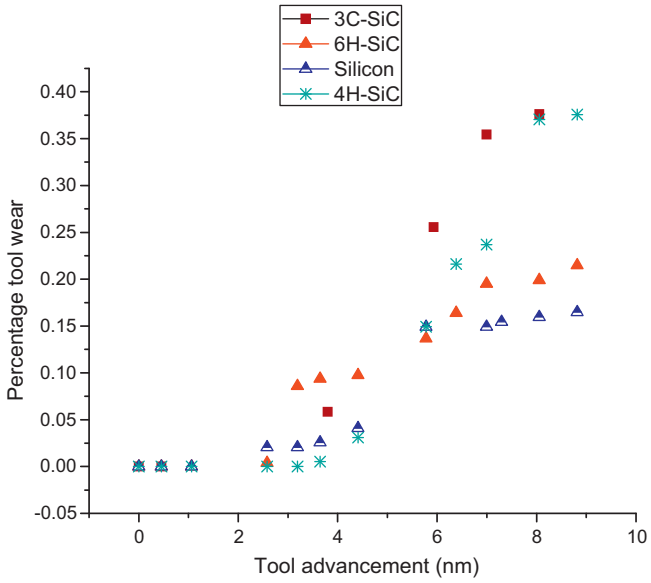

Fig. 12. Percentage tool wear of diamond tool.

of silicon carbide, albeit via a combined process of chemical and abrasion wear.[61]. Based on this, a novel, generic methodology to quantify tool wear from MD simulations using the change in coordination number has been recently reported by the authors.[49] The evolution of the percentage tool wear for all the cases using this approach is plotted in Fig. 12.

Fig. 12 suggest that the most rapid wear will occur while cutting 3C-SiC and 4H-SiC, interestingly, that 6H-SiC will show the least wear among the polytypes of SiC, approaching that of silicon. The increasing order of wear seems reasonably in line with the fact that the cutting hardnesses of 3C-SiC and 4H-SiC were higher than 6H-SiC, although there is a significant drop to reach that of silicon.

4. Conclusions

An MD simulation model has been used to develop a quantitative and qualitative understanding of the single point diamond turning of various polytypes of SiC with reference to silicon.

The following conclusions can be drawn accordingly:

1. A relatively new parameter, "cutting hardness" indicates that 3C-SiC (~2.9 times that of silicon) offers the highest cutting resistance followed by 4H-SiC (~2.8 times silicon) and 6H-SiC (~2.1 times silicon).
2. The thrust forces observed while machining SiC were higher than the cutting forces, whereas the opposite was the case for silicon using the same cutting conditions.
3. Deformed chips were generated in all cases which indicate that ductile regime machining is possible on all polytypes of SiC as well as silicon. However, there was a significant variation in the indicated quality of finished surfaces and sub-surface crystal lattice deformed layer depths. The simulations indicated that 4H-SiC would produce the best sub-surface integrity followed by 3C-SiC, silicon and 6H-SiC. Thus,

despite showing the lowest cutting resistance, 6H-SiC indicates the worst sub-surface integrity of the polytypes studied.
4. Cutting temperatures on the tool and workpiece also indicated that 3C-SiC offered the most cutting resistance followed by 4H-SiC, 6H-SiC and silicon.
5. The RDF and development of carbon co-ordination number both indicated that diamond cutting tools would graphitize due to abrasion against all the polytypes studied. While 3C-SiC and 4H-SiC indicated a high volume of wear, 6H-SiC suggests intermediate tool wear but still somewhat higher than silicon.
6. Considering all the above findings, it is reasonable to conclude that two of the polytypes may be suitable for SPDT, 4H-SiC offering the same cutting resistance as 3C-SiC but providing a better surface with less tool wear. However, 6H-SiC offered about half the cutting resistance of 4H-SiC but generated a poorer surface. Thus, the choice between 6H-SiC and 4H-SiC would be dictated by the trade-off between machined surface quality and cost considerations.

It must be noted here that the conclusions on the nanometric machinability of 3C-SiC are valid only for single crystal 3C-SiC and not for polycrystalline SiC. In other work, it has been shown that both chemically vapour deposited (CVD) 3C-SiC and reaction bonded (RB-SiC) are easier to machine than single crystal SiC.[73] This is because of the difference in the mechanism of chip formation between single crystal and polycrystalline SiC.

References

1. Ravindra D, Patten J. Improving the surface roughness of a CVD coated silicon carbide disk by performing ductile regime single point diamond turning. *ASME Conf Proc* 2008;**2008**(48517):155–61.
2. Patten JA. Chapter 2: Numerical simulations and cutting experiments on single point diamond machining of semiconductors and ceramics. In: Yan J, Patten JA, editors. *Semiconductor machining at the micro-nano scale*. Trivandrum-695 023, Kerala, India: Transworld Research Network; 2007.
3. http://www.grc.nasa.gov/WWW/SiC/, silicon carbide electronics. [accessed on 01.05.11].
4. Davies MA, Evans CJ, Patterson SR, Vohra R, Bergner BC. Application of precision diamond machining to the manufacture of micro-photonics components. In: *Lithographic and micromachining techniques for optical component fabrication II.* San Diego, USA: SPIE; 2003.
5. Blynsky, G., Closing in on perfection, in Fortune, 112[F]–112[L] - 23/06/2003.
6. Rhorer RL, Evans CJ. Fabrication of optics by diamond turning. In: *Handbook of Optics.* Mcgraw Hill; 2010.
7. Krauskopf B. Diamond turning: reflecting the demands of precision. *Manuf Eng* 1984;**92**:90–100.
8. Nakasuji T, Kodera S, Hara S, Matsunaga H, Ikawa N, Shimada S. Diamond turning of brittle materials for optical components. *CIRP Ann Manuf Technol* 1990;**39**(1):89–92.
9. Patten JA. Ductile regime nanocutting of silicon nitride. In: *Proceedings ASPE 2000 Annual Meeting*. 2000. p. 106–9.
10. Yan J, Zhang Z, Kuriyagawa T. Mechanism for material removal in diamond turning of reaction-bonded silicon carbide. *Int J Mach Tools Manuf* 2009;**49**(5):366–74.
11. Saito TT. Machining of optics: an introduction. *Appl Opt* 1975;**14**(8):1773–6.
12. Perrone, D., Ph.D. Thesis, Process and characterisation techniques on 4H – silicon carbide, in Micronanotechnology. 2007, Politecnico di Torino: Torino.
13. Taylor A, Laidler DS. The formation and crystal structure of silicon carbide. *Br J Appl Phys* 1950;**1**(7):174.
14. Tao H. Ph.D. Thesis, Atomistic model for nanoscale ductile mode cutting of silicon wafers, in Mechanical Engineering, National University of Singapore, Singapore, 2004.
15. Shimojo F, Ebbsjo I, Kalia RK, Nakano A, Rino JP, Vashishta P. Molecular dynamics simulation of structural transformation in silicon carbide under pressure. *Phys Rev Lett* 2000;**84**(15):p3338.
16. Tse JS, Klug DD, Gao F. Hardness of nanocrystalline diamonds. *Phys Rev B* 2006;**73**(14):140102.
17. http://www.memsnet.org/material/siliconsibulk/ [accessed on 27.12.11].
18. Vashishta P, Kalia Rajiv K, Nakano A, Rino Jose P. Interaction potential for silicon carbide: a molecular dynamics study of elastic constants and vibrational density of states for crystalline and amorphous silicon carbide. *J Appl Phys* 2007;**101**(10):103515–612.
19. Jasinevicius RG, Duduch JG, Porto AJV. Investigation on diamond turning of silicon crystal – generation mechanism of surface cut with worn tool. *J Brazil Soc Mech Sci* 2001;**23**:241–52.
20. CREE material datasheet 2011.
21. Qian J, Daemen LL, Zhao Y. Hardness and fracture toughness of moissanite. *Diamond Relat Mater* 2005;**14**(10):1669–72.
22. Pharr Matt, Katoh Yutai, and Bei Hongben, Dependence of Fracture toughness on crystallographic orientation in single crystalline cubic (β) silicon carbide. www.imechanica.org [accessed on 08.02.12].
23. Pirouz P, Zhang M, et al. Transition from brittleness to ductility in SiC. *J Phys: Condens Matter* 2002;**14**(48):12929.
24. Brede M, Haasen P. The brittle-to-ductile transition in doped silicon as a model substance. *Acta Metall* 1988;**36**(8):2003–18.
25. Codreanu C, Avram M, Carbunescu E, Iliescu E. Comparison of 3C–SiC, 6H–SiC and 4H–SiC MESFETs performances. *Mater Sci Semicond Process* 2000;**3**(1–2):137–42.
26. Bhatnagar M, Baliga BJ. Comparison of 6H–SiC: 3C–SiC, and Si for power devices. *IEEE Trans Electron Devices* 1993;**40**(3): 645–55.
27. Ko G, Kim H-Y, Bang J, Kim J. Electrical characterizations of neutron-irradiated SiC Schottky diodes. *Korean J Chem Eng* 2009;**26**(1): 285–7.
28. Carlo, PhD Thesis, Process and characterisation techniques on 3C – silicon carbide, in Micronanotechnology. 2007, Politecnico di Torino: Torino.
29. Neudeck PG. SiC technology. In: Raton B, editor. *The VLSI handbook*. Florida: CRC Press and IEEE Press; 2000. pp. 6.1–6.24.
30. Yu M, Jayanthi CS, Wu SY. Geometric and electronic structures of graphitic-like and tubular silicon carbides: ab-initio studies. *Phys Rev B* 2010;**82**(7):075407.
31. Patten J, Gao W, Yasuto K. Ductile regime nanomachining of single-crystal silicon carbide. *J Manuf Sci Eng* 2005;**127**(3):522–32.
32. Patten J, Jacob J. Comparison between numerical simulations and experiments for single-point diamond turning of single-crystal silicon carbide. *J Manuf Process* 2008;**10**:28–33.
33. Ravindra D, Patten JA. Chapter 4: Ductile regime material removal of silicon carbide, (SiC). In: Vanger SH, editor. *Silicon carbide: new materials, production methods and application*. Trivandrum, India: Nova Publishers; 2011. p. 141–67.
34. Belak JF, Stowers IF, Boercker DB. Simulation of Diamond turning of silicon surfaces. In: *Proceedings of 7th American Society Precision Engineering Annual conference*. 1992. p. 76–9.
35. Rentsch R, Inasaki I. Effects of fluids on the surface generation in material removal processes – molecular dynamics simulation. *CIRP Ann Manuf Technol* 2006;**55**(1):601–4.
36. Komanduri R, Raff L. A review on the molecular dynamics simulation of machining at the atomic scale. *Proc Inst Mech Eng B J Eng Manuf* 2001;**215**(12):1639–72.
37. Cai MB, Li XP, Rahman M. Study of the temperature and stress in nanoscale ductile mode cutting of silicon using molecular dynamics simulation. *J Mater Process Technol* 2007;**192–193**:607–12.
38. Goel S, Luo X, Reuben RL, Rashid WB. Replacing diamond cutting tools with CBN for efficient nanometric cutting of silicon. *Mater Lett* 2012;**68**(0):507–9.

39. Pen HM, Liang YC, Luo XC, Bai QS, Goel S, Ritchie JM. Multiscale simulation of nanometric cutting of single crystal copper and its experimental validation. *Comput Mater Sci* 2011;**50**(12):3431–41.
40. Plimpton S. Fast parallel algorithms for short-range molecular dynamics. *J Comput Phys* 1995;**117**:1–19.
41. Komanduri R, Chandrasekaran N, Raff LM. Molecular dynamics simulation of the nanometric cutting of silicon. *Philos Mag B* 2001;**81**(12): 1989–2019.
42. Cai MB, Li XP, Rahman M, Tay AAO. Crack initiation in relation to the tool edge radius and cutting conditions in nanoscale cutting of silicon. *Int J Mach Tools Manuf* 2007;**47**(3–4):562–9.
43. Promyoo R, El-Mounayri H, Yang X. molecular dynamics simulation of nanometric cutting. *Mach Sci Technol* 2010;**14**(4):423–39.
44. Zhang ZG, Fang FZ, Hu XT, Sun CK. Molecular dynamics study on various nanometric cutting boundary conditions. *J Vacuum Sci Technol B* 2009;**27**(3):1355–60.
45. Komanduri R, Chandrasekaran N, Raff LM. Effect of tool geometry in nanometric cutting: a molecular dynamics simulation approach. *Wear* 1998;**219**(1):84–97.
46. Tersoff J. Modeling solid-state chemistry: interatomic potentials for multicomponent systems. *Phys Rev B* 1989;**39**(8):5566.
47. Tersoff. Erratum: Modeling solid-state chemistry: interatomic potentials for multicomponent systems. *Phys Rev B* 1990;**41**(5):3248.
48. Humphrey W, Dalke A, Schulten K. VMD – visual molecular dynamics. *J Mol Graph* 1996;**14**:33–8.
49. Goel S, Luo X, Reuben RL. Molecular dynamics simulation model for the quantitative assessment of tool wear during single point diamond turning of cubic silicon carbide. *Comput Mater Sci* 2012;**51**(1):402–8.
50. Patten JA, Gao W. Extreme negative rake angle technique for single point diamond nano-cutting of silicon. *Precis Eng* 2001;**25**(2):165–7.
51. Goel S, Luo X, Goel G, Reuben R.L, Cutting hardness – an absolute measure after Mohs Hardness Scale. *Europhys lett*, submitted for publication.
52. Crompton D, Hirst W, Howse MGW. The wear of diamond. *Proc Roy Soc Lond Ser A: Math Phys Sci* 1973;**333**(1595):435–54.
53. Monnoye S, Turover D, Vicente P. In: Choyke WJ, Matsunami H, Pensl G, editors. *Surface preparation techniques for sic wafers silicon carbide*. Berlin Heidelberg: Springer; 2004. p. 699–710.
54. Belak J. Nanotribology: modelling atoms when surfaces collide. In: *Energy and Technology Review.* Lawrence Livermore Laboratory; 1994.
55. Yan J, Gai X, Harada H. Subsurface damage of single crystalline silicon carbide in nanoindentation tests. *J Nanosci Nanotechnol* 2010;**10**(11): 7808–11.
56. Lawn B, Wilshaw R. Indentation fracture: principles and applications. *J Mater Sci* 1975;**10**(6):1049–81.
57. Lawn BR, Marshall DB. Hardness, toughness, and brittleness: an indentation analysis. *J Am Ceram Soc* 1979;**62**(7-8):347–50.
58. Scattergood RO, Blake N. Ductile-regime machining of germanium and silicon. *J Am Ceram Soc* 1990;**73**(4):949–57.
59. Yan J. Laser micro-Raman spectroscopy of single-point diamond machined silicon substrates. *J Appl Phys* 2004;**95**(4):2094–101.
60. Domnich V, Gogotsi Y. phase transformations in silicon under contact loading. *Rev Adv Mater Sci* 2001;**3**(1.).
61. Goel S, Luo X, Reuben RL, Pen H. Influence of temperature and crystal orientation on tool wear during single point diamond turning of silicon. *Wear* 2012;**284–285**(0):65–72.
62. Tang, M. Ph.D. Thesis on elastic instabilities and structural responses of Beta-SiC under stress. Nuclear Engineering, Massachusetts Institute of Technology, Cambridge, Massachusetts, USA, 1995.
63. Szlufarska I, Kalia RK, Nakano A, Vashishta P. Atomistic mechanisms of amorphization during nanoindentation of SiC: a molecular dynamics study. *Phys Rev B* 2005;**71**(17.).
64. Noreyan A, Amar JG, Marinescu I. Molecular dynamics simulations of nanoindentation of beta-SiC with diamond indenter. *Mater Sci Eng B Solid State Mater Adv Technol* 2005;**117**(3):235–40.
65. Noreyan A, Amar JG. Molecular dynamics simulations of nanoscratching of 3C SiC. *Wear* 2008;**265**(7–8):956–62.
66. Yoshida M, Onodera A, Ueno M, Takemura K, Shimomura O. Pressure-induced phase transition in SiC. *Phys Rev B* 1993;**48**(14):10587–90.
67. Mishra M, Szlufarska I. Possibility of high-pressure transformation during nanoindentation of SiC. *Acta Mater* 2009;**57**(20):6156–65.
68. Goel S, Luo X, Reuben RL. Shear instability of nanocrystalline SiC during nanometric cutting (in press), App Phys Lett, 2012.
69. Bouwelen Van FM, Brown LM, Field JE. A new view on the mechanism of diamond polishing. *Ind Diamond Rev* 1997;**57**(1):21–5.
70. Karch K, Pavone P, Windl W, Schütt O, Strauch D. Ab initio calculation of structural and lattice-dynamical properties of silicon carbide. *Phys Rev B* 1994;**50**(23):17054–63.
71. Gogotsi YG, Kailer A, Nickel KG. Materials: transformation of diamond to graphite. *Nature* 1999;**401**(6754):663–4.
72. Yan J, Zhang Z, Kuriyagawa T. Effect of nanoparticle lubrication in diamond turning of reaction-bonded SiC. *Int J Automation Technol* 2011;**5**(3):307–12.
73. Goel S, Luo X, Stukowski A, Reuben RL. Influence of nanoparticle coolant and crystal structure of the workpiece during nanometric cutting of silicon carbide. In: *proceedings of the 12th EUSPEN International Conference*. Stockholm: EUSPEN; 2012.
74. http://hypertextbook.com/facts/2001/AliceWarrenGregory.shtml, Bond length [accessed 06.07.11].
75. Goel S, Luo X, Reuben RL, Rashid WB, Sun J. Single point diamond turning of single crystal silicon carbide: molecular dynamic simulation study. In: *Key Engineering Materials.* Liverpool: Key Engineering Materials; 2012. pp. 150–155.